AJNR

3D Cranial Nerve Imaging, a Novel MR Neurography Technique Using Black-Blood STIR TSE with a Pseudo Steady-State Sweep and Motion-Sensitized Driven Equilibrium Pulse for the Visualization of the Extraforaminal Cranial Nerve Branches

F. Van der Cruyssen, T.-M. Croonenborghs, R. Hermans, R. Jacobs and J. Casselman

AJNR Am J Neuroradiol published online 17 December 2020
http://www.ajnr.org/content/early/2020/12/17/ajnr.A6904

Published December 17, 2020 as 10.3174/ajnr.A6904

3D Cranial Nerve Imaging, a Novel MR Neurography Technique Using Black-Blood STIR TSE with a Pseudo Steady-State Sweep and Motion-Sensitized Driven Equilibrium Pulse for the Visualization of the Extraforaminal Cranial Nerve Branches

F. Van der Cruyssen, T.-M. Croonenborghs, R. Hermans, R. Jacobs, and J. Casselman

ABSTRACT

SUMMARY: This study investigated the feasibility of a 3D black-blood STIR TSE sequence with a pseudo steady-state sweep and motion-sensitized driven equilibrium pulse for extraforaminal cranial nerve imaging on a 3T system. Assessments of healthy volunteers showed near-perfect agreement in nerve visualization with excellent to good visualization of the extraforaminal trigeminal, greater occipital, and facial nerves. Suppression of surrounding tissues was excellent to good. 3D cranial nerve imaging can produce nerve selective imaging of extraforaminal cranial and spinal nerve branches.

ABBREVIATIONS: 3D CRANI = 3D cranial nerve imaging; PSS = pseudo steady-state; MDSE = motion-sensitized driven equilibrium

Being the largest cranial nerve, the trigeminal nerve—more specifically, its inferior alveolar and lingual branches—is frequently damaged during dental, oral, and maxillofacial surgical procedures.[1] Moreover, it can be subject to myriad disease entities such as inflammatory, infectious, neoplastic, and congenital pathology. MR imaging has been widely applied to the visualization of cranial nerves.[2] Intracranial trajectories such as nuclear and supranuclear, as well as cisternal segments, can be well depicted on routine MR imaging sequences. The cisternal segment is typically visualized using constructive interference in steady state and 3D heavily T2WI.[3] However, visualization of the extracranial peripheral branches on 3D T2WI remains a challenge because of their small diameters, tortuous courses, movement and susceptibility artifacts, and the presence of blood vessels in close proximity, which can all confound nerve visualization.[4] B1 and B0 inhomogeneities further lead to poor fat suppression and low SNR, and the use of multiple echoes to improve water and fat separation increases acquisition times considerably, making patient compliance difficult. To address these problems, we developed a novel black-blood 3D STIR TSE sequence for extraforaminal cranial nerve imaging (3D CRANI) on a 3T system and here describe its assessment.

Received April 7, 2020; accepted after revision September 18.

From the Departments of Oral & Maxillofacial Surgery (F.V.d.C., T.-M.C.) and Radiology (R.H.), University Hospitals Leuven, Leuven, Belgium; bOMFS-IMPATH Research Group (F.V.d.C., T.-M.C., R.J.), Department of Imaging and Pathology, Faculty of Medicine, University of Leuven, Leuven, Belgium; Department of Dental Medicine (R.J.), Karolinska Institutet, Stockholm, Sweden; Department of Radiology (J.C.), AZ St-Jan Brugge-Oostende, Bruges, Belgium; and Department of Radiology (J.C.), AZ St-Augustinus, Antwerp, Belgium.

Please address correspondence to Fréderic Van der Cruyssen, Department of Oral & Maxillofacial Surgery, University Hospitals Leuven, Kapucijnenvoer 33, 3000 Leuven, Belgium; e-mail: frederic.vandercruyssen@uzleuven.be

Indicates open access to non-subscribers at www.ajnr.org

Indicates article with online supplemental data.

http://dx.doi.org/10.3174/ajnr.A6904

Description of Technique

The 3D CRANI is a 3D TSE STIR black-blood sequence that uses a pseudo steady-state (PSS) sweep in combination with a motion-sensitized driven equilibrium (MSDE) pulse. We used STIR in combination with MSDE to ensure that signals from fat, muscle, and blood are suppressed uniformly across the field of view. The PSS sweep is designed such that the signal is smoothly varying during a long TSE shot to keep the signal strength approximately constant. This means that the flip angle sweep is not calculated based on specific tissue parameters (T1, T2). In this manner, it helps us to reduce the T2 decay for a range of tissues, which makes the sequence less sensitive to tissue dependencies. For the PSS functionality, minimum, middle, and maximum angles need to be defined, and 4 intermediate flip angles are used to asymptotically approach the minimum flip angle defined within the sequence (Online Supplemental Data). After reaching the minimum angle, nonlinear interpolation is used to calculate an optimum sweep according to the PSS principle while trying to keep the signal constant.[5] The middle angle is defined at the specified effective TE. After definition of the middle angle, the refocusing angles are increased linearly to the maximum defined angle.

Finally, compressed sensing is added to reduce the acquisition time. The sequence was optimized by comparing it with existing nerve-selective sequences until satisfactory and robust results were obtained, with particular attention being paid to artifact reduction (Online Supplemental Data).

MR Imaging Procedure

After optimization, 6 healthy volunteers (3 women and 3 men; average age, 32 years; range, 23–48 years) were included in this study. Imaging was performed on a 3T MR imaging system (Ingenia; Philips Healthcare) equipped with a 32-channel head coil (Invivo) without the use of any contrast agent. After acquisition of standard T1WI, T2WI, and gradient-echo sequences, the CRANI sequence was acquired using the following parameters: TR = 2300 ms, TE = 150 ms, FOV = 200 × 200 × 100 mm, section thickness = 0.5 mm, act section gap = −0.45 mm, matrix = 224 × 222, acquired voxel size = 0.9 × 0.9 × 0.9 mm, reconstructed voxel size = 0.5 × 0.5 × 0.45 mm, section oversampling = 1.5, compressed sense reduction = 5, and number of slices = 200. TSE nerve STIR included TSE factor = 45 (startup echoes 2), number of acquisitions = 1, black-blood pulse = MSDE (mode: nerve), and acquisition time = 5:17 min.

Weighted kappa scores, confidence intervals, and *P* values for the interobserver agreement for the observed variables

Parameter	Weighted Kappa Score	95% Confidence Interval	*P* Value
Arterial suppression	1	1–1	.014
Venous suppression	1	1–1	.014
Fat suppression	1	1–1	.014
Overall nerve visualization	1	1–1	.014
Inferior alveolar nerve	1	1–1	.014
Lingual nerve	1	1–1	.014
Facial nerve	0.933	0.79–1.10	.020
Greater occipital nerve	1	1–1	.014

Imaging Analysis

Three orthogonal planes, as well as a plane following the course of the nerve trajectory using MPR and MIP, were reconstructed using the Volume postprocessing package (Philips Healthcare). MIP images with a thickness of 5 mm and gap of −0.5 mm (4.5-mm overlap) allowed for the best demonstration of the selected nerve trajectory. The images were analyzed by 2 fixed and independent observers with expertise in cranial nerve imaging. First, a training session was held to familiarize the observers with the grading scales. Then, for the subsequent evaluations, the observers were blinded to each other's scoring. Arterial, venous, and fat suppression were graded on a 3-point Likert scale (0 = unsuppressed and nondiagnostic; 1 = moderately suppressed but diagnostic; 2 = excellent suppression). A nerve scoring system using a 5-point Likert scale (4 = excellent; 3 = good; 2 = fair;1 = poor; 0 = none) was adopted from Fujii et al[6] to evaluate the signal continuity of the following nerves over a predetermined trajectory. The evaluated trajectory of the inferior alveolar (V3) and lingual (V3) nerves starts at the oval foramen and stops at the mental foramen and the submandibular duct, respectively. The facial nerve (VII) trajectory starts in the labyrinthine portion in the temporal bone and stops at the anterior edge of the parotid. The greater occipital nerve (C2–C3) trajectory starts posterior to the axis and stops before piercing the trapezius muscle.[6]

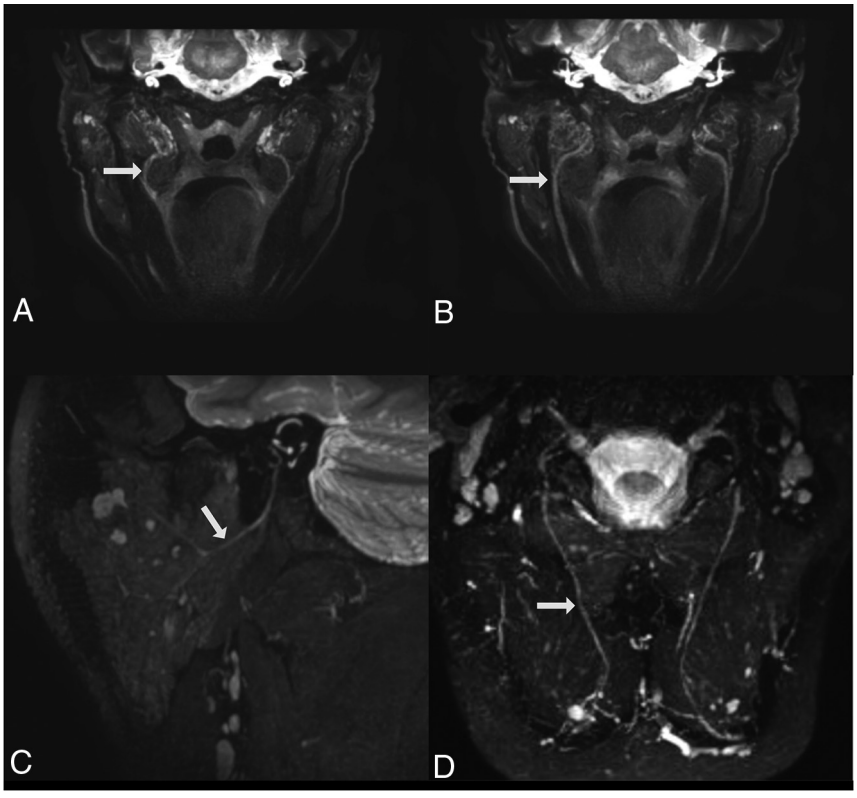

FIGURE. The evaluated cranial and spinal nerve branches acquired using the 3D CRANI sequence. *A*, Lingual nerve (*arrow*) on MIP after MPR. *B*, Inferior alveolar nerve (*arrow*) after MIP MPR on a coronal oblique reconstruction. *C*, Extraforaminal facial nerve (*arrow*) after sagittal oblique MIP MPR, illustrating the intraparotid nerve course. *D*, Greater occipital nerve (*arrow*) extending between the semispinalis muscles on MIP MPR.

Statistical Analysis

All statistical analyses were performed using SPSS version 26.0 (IBM). Interobserver agreement on the Likert scales was tested using weighted kappa statistics with quadratic weights. A *P* value less than .05 was considered statistically significant.

RESULTS

There was a statistically significant near-perfect agreement between the 2 observers, except in the visualization of the extracranial portion of the facial nerve, for which the agreement was still

considered to be very good (independent observer scores are illustrated in the Online Supplemental Data). The strength of agreement ranged from very good to excellent for all parameters (Table). Venous suppression was evaluated as excellent except in 2 cases in which it was considered "moderately suppressed." These 2 cases also had the lowest scores for the other variables observed. When the independent nerve scoring results were evaluated, the facial nerve had the lowest scores. The visualizations of the trigeminal and greater occipital nerve branches were rated as good to excellent. The Figure illustrates the nerve-selective sequence with examples of the evaluated structures.

DISCUSSION

This technical note successfully demonstrates the use of 3D CRANI, a modified black-blood STIR TSE sequence for nerve-selective imaging of peripheral cranial and spinal nerve branches. Diffusion-weighted prepulsing by MSDE for MR neurography purposes was first described by Yoneyama et al[7] and further demonstrated for brachial plexus imaging by Klupp et al.[8] This study is innovative in the sense that an MSDE pulse was applied in combination with a PSS sweep to further optimize nerve-enhanced imaging within clinically feasible acquisition times. The results from our study indicate excellent interobserver agreement. Moreover, the scoring of the images indicates moderate to excellent suppression of surrounding tissues. Chhabra et al[9,10] published several papers on cranial nerve imaging and advocate several sequences for clinical evaluations, including a STIR TSE sequence when magnetic field inhomogeneities are expected.[11,12] However, their main imaging method for MR neurography involves diffusion-weighted reversed fast imaging with steady-state free precession, which is applied using gradient-echo imaging. In the past, gradient-echo imaging was preferred because of its short acquisition times. However, with new techniques such as those illustrated in this study, STIR sequences with reasonable acquisition times, low artifact susceptibility, and excellent fat suppression have become possible. The current limitations appear to be similar signal intensities for nerve and (intraparotid) lymphoid tissue, unpredictable visualization of nerves with a diameter less than 0.9 mm, and imperfect venous suppression of the pterygoid plexus. A future large prospective study will be designed to validate this sequence in both healthy and patient populations, comparing 3D CRANI with existing protocols.

CONCLUSIONS

3D CRANI can produce nerve-selective imaging of the trigeminal, facial, and greater occipital extraforaminal nerve branches, with excellent interobserver agreement and within clinically feasible acquisition times. Prospective studies are needed to further evaluate and validate its clinical use.

ACKNOWLEDGMENTS

The authors thank Marco Nijenhuis and Vermurugan Gnanaprakasam for their technical assistance and insights and Prof. Dr. Avneesh Chhabra for providing the initial PSIF sequence examination card. The authors also thank Dr. Ronald Peeters and Dr. Frederik De Keyzer for their continuous input and their work on the protocol optimization. The authors also thank Karl Embleton, PhD, from Edanz Group (https://en-author-services.edanzgroup.com/ac) for editing a draft of this manuscript.

Disclosures: Fréderic Van der Cruyssen—*UNRELATED: Employment:* UZ Leuven, *Comments*: Resident at University Hospitals Leuven, Belgium at the department of Oral & Maxillofacial Surgery. Jan Casselman—*UNRELATED: Consultancy:* Philips Healthcare, *Comments*: Customer visits*; *Payment for Lectures Including Service on Speakers Bureaus:* Philips Healthcare, *Comments*: Payment for lectures; *Travel/Accommodations/Meeting Expenses Unrelated to Activities Listed:* Philips Healthcare, *Comments*: Reimbursement travel for lectures given for Philips Healthcare. *Money paid to institution.

REFERENCES

1. Renton T, Van der Cruyssen F. **Diagnosis, pathophysiology, management and future issues of trigeminal surgical nerve injuries.** *Oral Surg* 2019;13:389–403 CrossRef
2. Romano N, Federici M, Castaldi A. **Imaging of cranial nerves: a pictorial overview.** *Insights Imaging* 2019;10:33 CrossRef Medline
3. Casselman J, Mermuys K, Delanote J, et al. **MRI of the cranial nerves—more than meets the eye: technical considerations and advanced anatomy.** *Neuroimaging Clin N Am* 2008;18:197–231 CrossRef Medline
4. Chhabra A, Madhuranthakam AJ, Andreisek G. **Magnetic resonance neurography: current perspectives and literature review.** *Eur Radiol* 2018;28:698–707 CrossRef Medline
5. Busse RF, Brau ACS, Vu A, et al. **Effects of refocusing flip angle modulation and view ordering in 3D fast spin echo.** *Magn Reson Med* 2008;60:640–49 CrossRef Medline
6. Fujii H, Fujita A, Yang A, et al. **Visualization of the peripheral branches of the mandibular division of the trigeminal nerve on 3D double-echo steady-state with water excitation sequence.** *AJNR Am J Neuroradiol* 2015;36:1333–37 CrossRef Medline
7. Yoneyama M, Takahara T, Kwee TC, et al. **Rapid high resolution MR neurography with a diffusion-weighted pre-pulse.** *Magn Reson Med Sci* 2013;12:111–19 CrossRef Medline
8. Klupp E, Cervantes B, Sollmann N, et al. **Improved brachial plexus visualization using an adiabatic iMSDE-prepared STIR 3D TSE.** *Clin Neuroradiol* 2019;29:631–38 CrossRef Medline
9. Chhabra A, Andreisek G, Soldatos T, et al. **MR neurography: past, present, and future.** *AJR Am J Roentgenol* 2011;197:583–91 CrossRef Medline
10. Chhabra A, Padua A Jr, Flammang A, et al. **Magnetic resonance neurography—techniques and interpretation.** *Magnetom Flash-Clin Neurol* 2012;2:4–8
11. Zuniga JR, Mistry C, Tikhonov I, et al. **Magnetic resonance neurography of traumatic and nontraumatic peripheral trigeminal neuropathies.** *J Oral Maxillofac Surg* 2018;76:725–36 CrossRef Medline
12. Cox B, Zuniga JR, Panchal N, et al. **Magnetic resonance neurography in the management of peripheral trigeminal neuropathy: experience in a tertiary care centre.** *Eur Radiol* 2016;26:3392–400 CrossRef Medline